A&A 371, 1128–1136 (2001)
DOI: 10.1051/0004-6361:20010464

Astronomy & Astrophysics

Investigation of temperature and velocity fluctuations through the solar photosphere with the Na I D lines

M. T. Eibe[1], P. Mein[1], Th. Roudier[2], and M. Faurobert[3]

[1] DASOP, Observatoire de Paris, Section de Meudon, 92195 Meudon, France
e-mail: Pierre.Mein@obspm.fr
[2] Laboratoire d'Astrophysique de Toulouse, Observatoire Midi-Pyrénées, 14 avenue E. Belin, 31400 Toulouse, France
e-mail: thierry.roudier@bagn.obs-mip.fr
[3] Observatoire de la Côte d'Azur, BP 4229, 06304 Nice Cedex 04, France
e-mail: faurob@obs-nice.fr

Received 26 January 2001 / Accepted 7 March 2001

Abstract. In this work we explore the diagnostic properties of the Na I D resonance lines by calculating the response functions of their line profiles to temperature and velocity perturbations in the atmosphere. We propose a method to transform spectral line intensity fluctuations measured at several wavelengths into temperature and velocity disturbances at different height levels. Results from tests done with several theoretical models of perturbations are discussed. Perturbations that vary as linear functions of depth are efficiently reproduced. The method also provides good estimations for exponential models. As an example we present an application to solar granulation data obtained with Multichannel Subtractive Double Pass (MSDP) spectroscopy.

Key words. line: profile – Sun: photosphere – Sun: granulation

1. Introduction

Two-dimensional high resolution spectroscopic observations of the solar surface are now available. Intensity and velocity maps of the observed field of view can be produced at high spatial resolution. High spatial resolution in the vertical direction may be also achieved by measuring the spectral line profile at various wavelength positions simultaneously. To exploit such high quality data, a good knowledge of the spectral line formation is required. For a correct interpretation of results it is very important to locate the atmospheric layers which are responsible for intensity variations at the observed wavelengths.

The Na I D resonance doublet is a good diagnostic of the solar photosphere. Both D_1 and D_2 lines show strong and well extended wings, allowing us to probe a wide range of atmospheric heights.

In this paper we investigate the mapping between given wavelengths in the D line profiles and atmospheric height levels. Our approach involves calculation of Response Functions, which are classical tools for inversion techniques. We aim to convert fluctuations of intensity and Doppler velocity as measured from spectrograms into atmospheric disturbances of temperature and macroscopic velocity, respectively, at characteristic heights. This kind of analysis is very important to clarify the structure and dynamics of photospheric layers. Results can also be used to evaluate theoretical models of solar granulation. In addition, physical properties of deep convective layers are often used as boundary conditions in the study of solar interior phenomena.

The theoretical basis of our method is explained in Sect. 2. Temperature and velocity Response Functions are discussed in Sect. 3. As an illustrative example we present an application to solar granulation data in Sect. 4. A summary and conclusions are given in Sect. 5.

Send offprint requests to: M. T. Eibe,
e-mail: Teresa.Eibe@obspm.fr

2. Method

The calculation of so-called Response Functions to temperature and macroscopic velocity for the Na D line profiles constitutes the essential part of this method. We briefly introduce the concept of Response Functions below and explain in detail how they were calculated.

Their use in the analysis of observational data to estimate physical conditions will be described at the end of the section.

2.1. Calculation of response functions

Response Functions (hereafter, *RF*s) describe the effect that perturbations of a given physical parameter have in the emergent line intensity (Mein 1971; Beckers & Milkey 1975; Canfield 1976; Caccin et al. 1977). In the past years they have become extensively used for the inversion of line profiles and Stokes spectra (Ruiz Cobo & del Toro Iniesta 1992; Bellot Rubio et al. 1997). By means of *RF*s one can estimate the heights of formation for measurements that are obtained from observed quantities (Sánchez Almeida et al. 1996). If $RF_{\rm p}$ is the response function for a certain parameter, p, the intensity fluctuation that corresponds to a small disturbance Δp, can be written as

$$\Delta I(\lambda) = \int_0^{+\infty} RF_{\rm p}(\lambda, s)\, \Delta p(s)\, {\rm d}s, \tag{1}$$

where s is the coordinate associated to atmospheric height.

*RF*s of the D_2 line have been obtained before for temperature, velocity and pressure fluctuations under LTE conditions (Kneer & Nolte 1994; Krieg et al. 1999; Krieg et al. 2000).

The version 2.2 of the non-LTE radiative transfer code MULTI (Carlsson 1986) was used in this work to compute theoretical fluctuations of intensity which are caused by temperature and velocity perturbations in the atmosphere. Atomic data and $D_{1,2}$ transition parameters for input in MULTI were taken from the Na I model atom given by Bruls et al. (1992), considering 10 bound levels and the ground state of Na^+. The MULTI code uses the simplification of complete frequency redistribution of photons (CRD), which is well justified in the case of the D lines (Kelch & Milkey 1976). In the CRD approximation, absorption and re-emission of photons are frequency-independent processes. As a result, the emission profile equals the absorption profile and the source function is independent of frequency (Mihalas 1978). This simplifies considerably the treatment of radiative transfer problems.

As the standard Na I $D_{1,2}$ line profiles, $I_{\rm st}$, we use those obtained for the reference VAL C mean quiet-sun model atmosphere (Vernazza et al. 1981). A set of theoretical profiles was next computed for small departures from the reference model atmosphere. A given profile, $I_{\rm i}(\lambda)$, corresponds to a model atmosphere which has been locally disturbed at all depths contained in the interval defined by the starting bottom point, s_0, and an upper limit $s_{\rm i}$. The depth $s_{\rm i}$ is varied sequentially from bottom to top through the 97 depth points of the model atmosphere, resulting therefore in 97 synthetic profiles. The subsequent intensity fluctuations for a small perturbation affecting a depth interval $[s_{\rm i}, s_{\rm i} + \Delta s]$ can then be obtained as

$$\delta I_{\rm i}(\lambda) = (I_{\rm i+1}(\lambda) - I_{\rm st}(\lambda)) - (I_{\rm i}(\lambda) - I_{\rm st}(\lambda)). \tag{2}$$

The term $I_{\rm st}(\lambda)$ may be removed in the equation above as it is cancelled out in the subtraction.

Temperature perturbations are introduced as a change of the local value by the factor $(1 + \Delta T/T)$, where $\Delta T/T$ is fixed and equal to 0.01, sufficiently small for the subsequent variation to be treated as a linear perturbation. In the case of velocity, absolute perturbations are used with a constant value of $V = 0.125$ km s^{-1}.

Temperature response functions, $RF_{\rm T}$, can then be calculated as

$$RF_{\rm T}(\lambda, s_{\rm i}) = \frac{\delta I_{\rm i}(\lambda)}{\frac{\Delta T}{T} I_{\rm c} \Delta s}. \tag{3}$$

In this expression we have considered intensity fluctuations relative to continuum intensity, $I_{\rm c}$, for convenience.

In the case of velocity response functions, $RF_{\rm V}$, we use the difference of intensity fluctuations in the blue and in the red part of the profile to derive Doppler shifts. Thus, for positions in the line which are symmetrical to line centre: $\lambda_+ = \lambda_{\rm c} + \Delta\lambda_{\rm i}$, $\lambda_- = \lambda_{\rm c} - \Delta\lambda_{\rm i}$, being $\lambda_{\rm c}$ the wavelength of the line centre, we obtain:

$$\Delta I_{\pm,{\rm i}} = (I_{\rm i}(\lambda_+) - I_{\rm st}(\lambda_+)) - (I_{\rm i}(\lambda_-) - I_{\rm st}(\lambda_-)). \tag{4}$$

Intensity fluctuations calculated in this way for each synthetic profile are directly related to velocity by:

$$\Delta I_{\pm,{\rm i}} \simeq \frac{{\rm d}I}{{\rm d}\lambda} 2\lambda_{\rm c} \frac{V}{c}.$$

Fluctuations caused by local perturbations of velocity, $\delta I_{\pm,{\rm i}}$, are approximated by residual intensities as before (Eq. (2)). The expression for $RF_{\rm V}$ is then:

$$RF_{\rm V}(\lambda, s_{\rm i}) = \frac{\delta I_{\pm,{\rm i}}(\lambda)}{V \Delta s} = \frac{\Delta I_{\pm,{\rm i+1}} - \Delta I_{\pm,{\rm i}}}{V \Delta s}. \tag{5}$$

As a depth scale we have chosen the logarithm of column mass, i.e. $s \equiv \log m$. Model atmospheres start at $\log m = 0.75$ and run up to $\log m = -5.28$ (m is in units of g cm^{-2}). It is assumed that perturbations occurring at depths larger than $\log m = 0.75$ have no effect at all in the profile. The advantage of using column mass as the depth variable is that, in conditions of hydrostatic equilibrium, it is directly related to pressure. In this way the vertical stratification is preserved, even after temperature or velocity disturbances have been introduced. The geometrical height, however, would vary according to the way perturbations affect opacity and would need to be recalculated specifically for each perturbed atmosphere. The geometrical height scale that is used for reference in the plots is calculated for the static unperturbed atmosphere so that the origin $h = 0$ corresponds to the level at which standard optical depth is 1, increasing outwards.

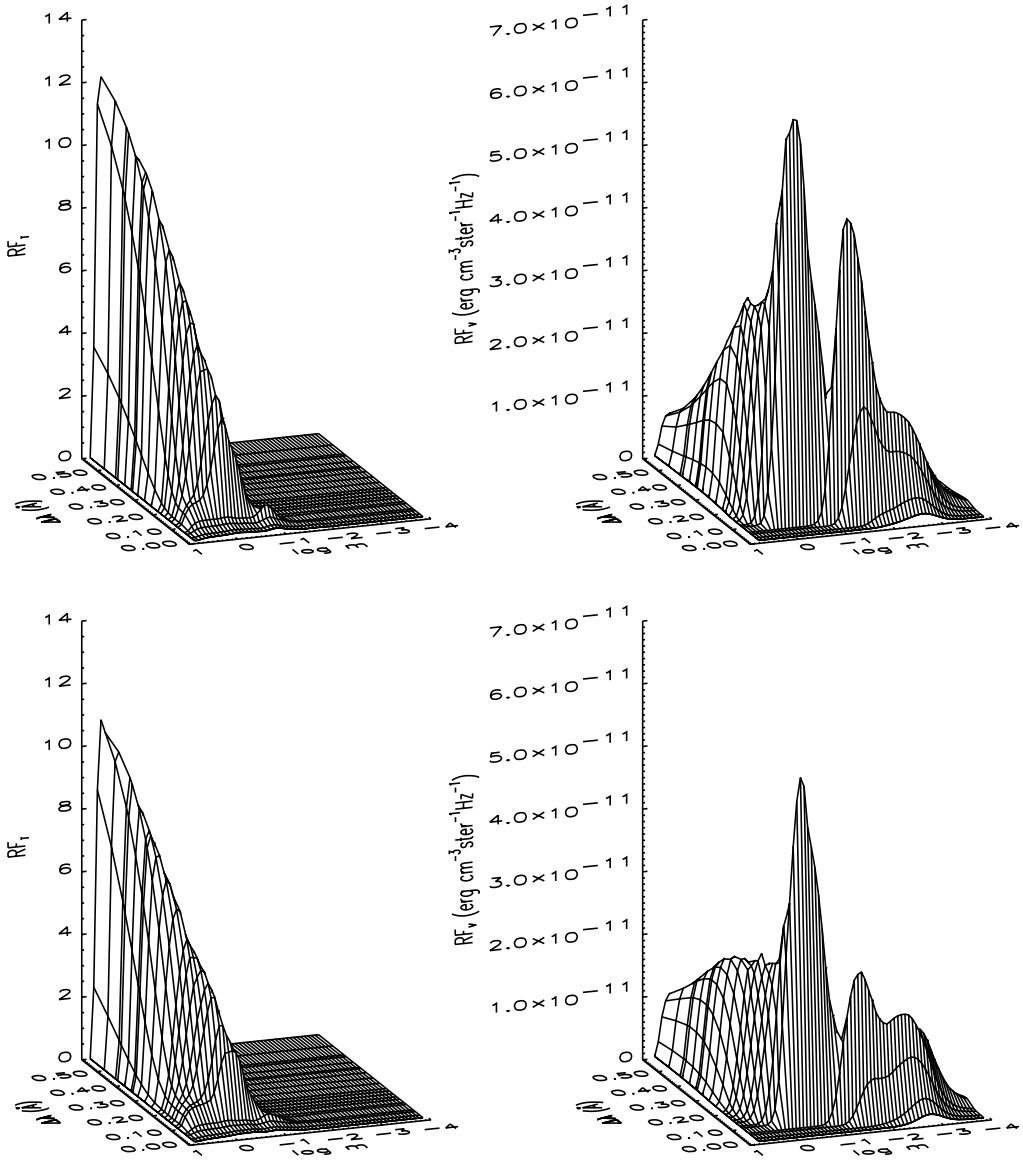

Fig. 1. *RF*s of the Na I D_1 (top panel) and D_2 (bottom panel) lines for temperature (left) and for velocity (right). The "x" axis refers to wavelength distance from line centre. For clarity, the negative side of the axis is not plotted since the *RF*s are symmetrical with respect to $\Delta\lambda = 0$. Depth is indicated in the "y" axis as $\log m$, where m is column mass in $\mathrm{g\,cm^{-2}}$ (see text)

2.2. Estimation of temperature and velocity with RFs

Barycenters of *RF*s for different wavelengths, $G(\lambda)$, give an indication for depths at which relevant perturbations occur. They are defined as:

$$G(\lambda) = \frac{\int_0^{+\infty} RF(\lambda, s) s \, \mathrm{d}s}{\int_0^{+\infty} RF(\lambda, s) \, \mathrm{d}s}. \tag{6}$$

Barycenters are also of interest because they allow one to estimate perturbation amplitudes at different levels in the atmosphere. If we assume that perturbations vary linearly with depth (i.e., $\Delta p(s) = A + Bs$), then the observed intensity (or velocity) fluctuations at wavelength λ, together with the barycenter of the *RF* for that wavelength, $G(\lambda)$, will provide the perturbation value at the barycenter height.

In the case of temperature this can be written as:

$$\begin{aligned} \frac{\Delta I(\lambda)}{I_\mathrm{c}} &= \int_0^{+\infty} (A + Bs) RF_\mathrm{T} \, \mathrm{d}s \\ &= \left(\frac{\Delta T}{T}\right)_{s=G(\lambda)} \int_0^{+\infty} RF_\mathrm{T} \, \mathrm{d}s. \end{aligned}$$

As a result,

$$\left(\frac{\Delta T}{T}\right)_{s=G(\lambda)} = \frac{\Delta I_\mathrm{obs}(\lambda)}{\int_0^{+\infty} RF_\mathrm{T}(\lambda, s) \, \mathrm{d}s}. \tag{7}$$

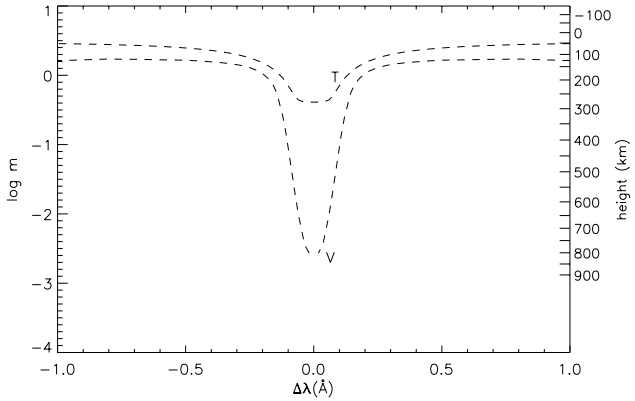

Fig. 2. Variation of $RF_{\rm T}$ and $RF_{\rm V}$ barycenters with depth for the D_1 line

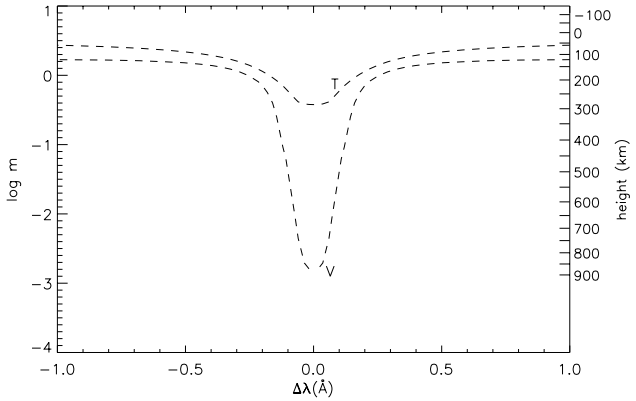

Fig. 3. As Fig. 2 but for the D_2 line

Analogously, the calculation of velocity disturbances from observed fluctuations and for the heights of formation given by barycenters would be as follows:

$$\Delta V(\lambda) = \frac{c}{\frac{\mathrm{d}I}{\mathrm{d}\lambda} 2\lambda_{\rm c}} \int_0^{+\infty} (A + Bs) RF_{\rm V}\, \mathrm{d}s.$$

In this way, the velocity disturbance at the barycenter height can be derived as:

$$V_{s=G_\lambda} = \frac{\Delta V_{\rm obs}}{\frac{c}{\frac{\mathrm{d}I}{\mathrm{d}\lambda} 2\lambda_{\rm c}} \int_0^{+\infty} RF_{\rm V}\, \mathrm{d}s}. \qquad (8)$$

3. Results

3.1. Temperature response functions

RFs for temperature, $RF_{\rm T}$, were derived using Eq. (3) with $\frac{\Delta T}{T} = 0.01$. Results are shown in Fig. 1. The wavelength scale in the x-axis covers only one side of the profile, for the sake of clarity. However, one should keep in mind that RFs are symmetrical with respect to the axis $\Delta\lambda = 0$.

Figures 2 and 3 show the barycenter distribution with height for $RF_{\rm T}$ at different wavelengths in the D_1 and D_2 lines, respectively. The barycenter shifts progressively from the lower photosphere in the far wings of the line to heights up to 280 km near the centre of the line. The computed barycenters of $RF_{\rm T}$ for a sample of wavelength positions in the D profiles can be found in Tables 1 and 2. The conversion factors between observed fluctuations and actual perturbations of the atmospheric model,$(\frac{\Delta I}{I})/(\frac{\Delta T}{T})$, deduced with Eq. (7), are also included for each wavelength.

There are not large differences between results obtained for D_1 and D_2. $RF_{\rm T}$ for D_1 tend to shift towards lower heights. This is consistent with the fact that this line shows less pronounced wings in comparison to D_2. In all cases $RF_{\rm T}$ show a well defined peak over a certain interval of height, depending on which wavelength we consider in the line profile. This defines the atmospheric layers which contribute most to the observed variations of emergent intensity. By using observations at appropriate wavelengths we may better resolve the vertical structure of temperature. In general, the line profile will be more sensitive to disturbances at large depths. The depth limit above which disturbances have a negligible effect is at $\log m = -2$. This corresponds to a height of 650 km in the VAL C model.

In order to verify linearity, we calculated $RF_{\rm T}$ in the case of $\Delta T/T = 0.02$ and we compared it with those for $\Delta T/T = 0.01$. As expected in a linear regime, the amplitude of the resulting intensity fluctuations is two times greater for $\Delta T/T = 0.02$, within an error $\lesssim$5%. Consequently, the $RF_{\rm T}$ behaviour is the same in both cases.

Table 1. $RF_{\rm T}$ and $RF_{\rm V}$ barycenters ($G(\lambda)$ in Eq. (6)) in $\log m$ and height [km] coordinates for the Na I D_1 line. The last two columns are for the conversion factors between relative intensity fluctuations and perturbations at the barycenter heights, which are derived with Eqs. (7) and (8) on the assumption of constant vertical gradient

$\Delta\lambda$	$RF_{\rm T}$bar.		$RF_{\rm V}$bar.		$\frac{\Delta I}{I}/\frac{\Delta T}{T}$	$\frac{\Delta I_\pm}{I}/V$
(Å)	$\log m$	h	$\log m$	h		
0.072	–0.31	260	–1.73	577	7.80	1.75
0.108	–0.09	206	–0.84	381	7.85	0.64
0.120	–0.04	192	–0.60	327	8.22	0.36
0.144	0.05	170	–0.26	247	8.78	0.21
0.180	0.14	145	–0.04	145	9.08	0.16
0.216	0.21	127	0.06	167	8.98	0.12
0.252	0.25	114	0.11	153	8.67	0.10
0.288	0.29	103	0.14	144	8.27	0.08
0.324	0.32	95	0.17	138	7.88	0.06
0.360	0.34	89	0.18	134	7.51	0.05
0.432	0.37	79	0.21	127	6.92	0.03

3.2. Velocity response functions

Figure 1 shows velocity RFs, $RF_{\rm V}$, calculated with $V = 0.125$ km s^{-1} in Eq. (5). As opposed to $RF_{\rm T}$, $RF_{\rm V}$ are not always negligible at heights larger than $\log m = -2.0$. The maximum contribution for both D_1 and D_2 lines is

Table 2. As Table 1 but for the Na I D_2 line

$\Delta\lambda$ (Å)	RF_T bar. $\log m$	h	RF_V bar. $\log m$	h	$\frac{\Delta I}{I}/\frac{\Delta T}{T}$	$\frac{\Delta I_\pm}{I}/V$
0.072	–0.34	267	–2.05	657	7.50	1.44
0.108	–0.20	232	–1.21	459	8.03	0.72
0.120	–0.15	221	–1.03	421	8.23	0.37
0.144	–0.08	202	–0.60	327	8.50	0.19
0.180	0.02	179	–0.25	245	8.84	0.14
0.216	0.09	160	–0.09	206	9.07	0.12
0.252	0.15	144	–0.01	185	9.16	0.11
0.288	0.19	131	0.05	170	9.08	0.09
0.324	0.23	120	0.09	160	8.89	0.08
0.360	0.26	112	0.12	152	8.63	0.06
0.432	0.31	98	0.16	141	8.05	0.05

found for $\Delta\lambda = 0.108$ Å at heights close to $\log m = -0.5$ (∼290 km).

The plots for RF_V barycenters (Figs. 2 and 3) confirm that RF_V cover a larger range of heights than RF_T. With RF_V one can obtain information for heights up to $\log m \sim -2.8$ (geometrical height of 900 km). As in the case of temperature, we will observe deeper as we move to the wings in the line profile. Tables 1 and 2 show the barycenters obtained for RF_V at the same wavelengths as given for temperature. The conversion factors that are required to transform observed fluctuations into velocity perturbations, $(\frac{\Delta I_\pm}{I})/V$, are also included.

In order to test linearity we have calculated RF_V with $V = 0.25$ km s^{-1} using the same procedure. The effect in the calculated fluctuations of intensity is doubled, as expected, with errors no larger than 3%, yielding the same result.

3.3. Tests with theoretical models

Confidence in results from the calculated RFs may be explored through theoretical profiles obtained for known models of perturbations. With this aim, several atmospheric models were created by introducing small-amplitude temperature (or velocity) disturbances which may be described as either linear or natural exponential functions of depth. The D_2 line profiles computed for those models were then used to derive the values of disturbances at barycenter depths with the RFs as explained above. Figure 4 shows comparison of results (*crosses* for linear models and *dots* for exponential models) with the actual values for the corresponding models of perturbations (*continuous lines*). Each model is labelled in the plot with the parameter that determines the variation with height: the slope, b, for linear models ($b\log(m_0/m)$) and the factor α that defines natural exponential functions ($e^{\alpha\ln(m_0/m)}$).

In the case that perturbations are exponential functions of depth, it may be more convenient to represent results on a logarithmic scale, as shown in Figs. 5 and 6. The subscript "0" refers to the origin of geometrical height, at the level where standard optical depth is equal to 1

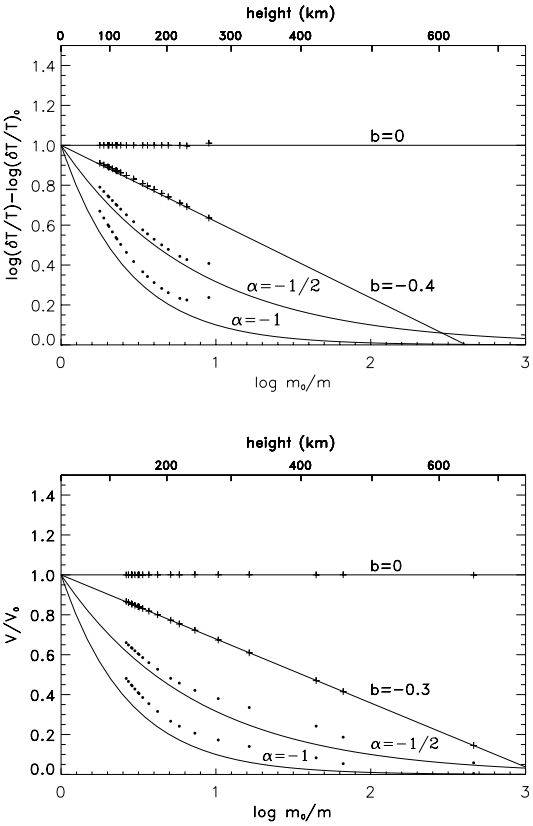

Fig. 4. Temperature (*upper panel*) and velocity (*lower panel*) fluctuations obtained with our method for assumed models of perturbations (*solid lines*). Each model is labelled in the plot with the parameter that determines the variation with height: the slope, b, for linear models ($b\log(m_0/m)$) and the factor α that defines natural exponential functions ($e^{\alpha\ln(m_0/m)}$). The corresponding values predicted with our method are indicated as crosses for linear models and dots for exponential models. Departures between curves and points increase for large values of $|\alpha|$, reflecting the fact that perturbations are far from linear functions of depth

($\tau_{5000} = 1$). Perturbation models that vary with height as exponential functions of the form $e^{\alpha\ln(m_0/m)}$ correspond to straight solid lines in the figures. Models predicted by our method are shown with dotted lines. It was checked that these results do not depend on the given value of the perturbation amplitude at $h = 0$, $(\delta T/T)_0$ or $(\delta V)_0$, as long as it is sufficiently small. The effect of doubling the amplitude results in very similar curves to those shown in Figs. 5 and 6. The differences are not larger than 3% for temperature perturbations and 10% for velocity perturbations.

Deviations between actual models and those predicted by the method are more important for larger absolute values of α. For these models the assumption of constant vertical gradient leads to larger errors through Eqs. (7) and (8). A second reason for the loss of accuracy is related to the fact that RFs extend over a certain range of heights. In the ideal case, RFs at a given wavelength would be δ-functions centred at one characteristic height. Assignment of atmospheric heights to measurements made

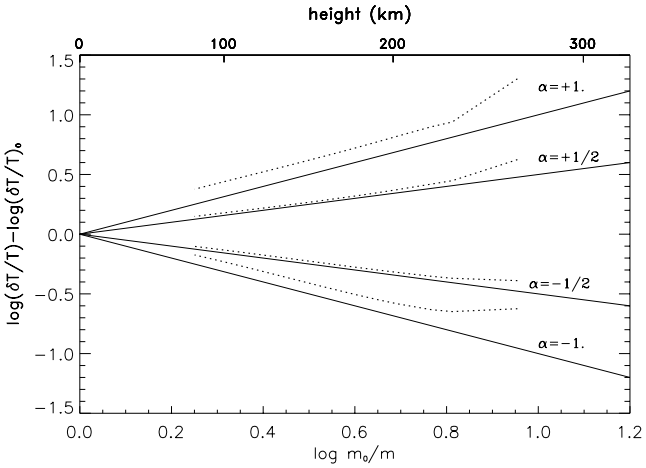

Fig. 5. Exponential models of perturbations plotted in logarithmic scale, so that $\log(\delta T/T) - \log(\delta T/T)_0 = \alpha(\log m_0/m)$, where the subscript "0" is for the origin of geometrical height, at the level where standard optical depth is equal to 1 ($\tau_{5000} = 1$). *Thick solid lines* are for the assumed models. Models predicted by our method are shown with *dotted lines*

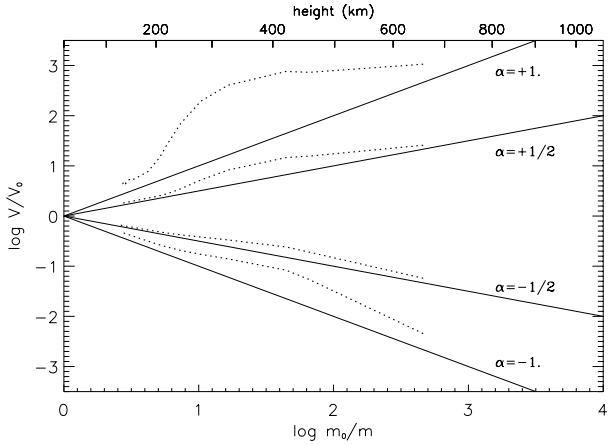

Fig. 6. As Fig. 5 but for exponential models of velocity perturbations: $\log(\delta V) - \log(\delta V)_0 = \alpha(\log m_0/m)$

at particular wavelengths would then be immediate. In practice, because RFs have a finite width, the observed fluctuations are actually weighted sums of contributions from several depths. This effect is particularly important for the line core velocity response functions, which show two distinct lobes (Fig. 7). As a result, physical perturbations in the atmosphere will be smeared out and height determinations will be more uncertain. As a consequence, large deviations between predicted and real values of perturbations are to be expected at larger heights.

Fits to the variation with height of temperature and velocity perturbations derived with this method can be done by direct comparison with Figs. 5 and 6. Predicted models (*dotted lines*) should be used as a reference to search for the exponential factor α giving the best fit. The amount of the vertical shift that must be applied in order to adjust results to that model would give the perturbation value at height 0.

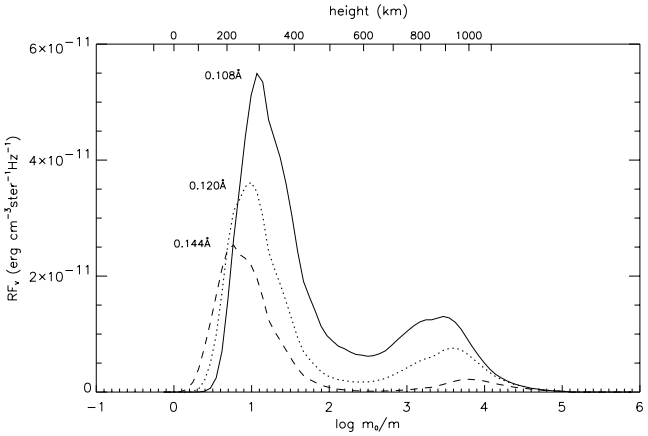

Fig. 7. Velocity RFs of the D_2 line profile at certain wavelength positions in the line core showing two distinct lobes as discussed in the text

4. An example with solar granulation data

We have used the method described in the previous section to investigate the vertical structure of solar granulation through the analysis of MSDP spectrograms in the Na D_2 line. The MSDP technique allows one to measure the line profile simultaneously for each position of the observed field of view. Two-dimensional maps of intensity and doppler velocity fluctuations can be produced for each of the observed wavelengths. Following our procedure we can derive the atmospheric perturbations of temperature and velocity that would be required to reproduce observations.

Observations were taken at the Coupole Tourelle in Pic du Midi Observatory in October 22, 1988. A temporal sequence of 64 2D spectrograms covering a quiet area of the solar surface was recorded in the Na I D_2 line (5890 Å) using the 50 cm refractor with the MSDP spectrograph, under excellent seeing conditions. The effective field of view after image processing is $172'' \times 8''$. The total duration of the sequence is 16 min, with consecutive frames separated by 15 s. Correction for the 5-min oscillations was done by filtering each frame in the $k-\omega$ plane (see Espagnet et al. 1995 for further instrumental details).

A statistical and morphological analysis of the same set of data was carried out by Espagnet et al. (1995) and Roudier et al. (2001). The behaviour of overshooting granules was investigated and a description of the vertical structure of the photosphere was provided, based on the observed fluctuations of intensity and velocity. Results were highly conditioned by the uncertainty associated with the height values, obtained as an average of the heights of formation for sodium lines calculated in previous works (Athay & Canfield 1969; Babij & Stodilka 1987).

A detailed study of the temporal evolution of exploding granules detected in the observations was done by Roudier et al. (2001). The height dependence of the associated temperature and velocity disturbances through

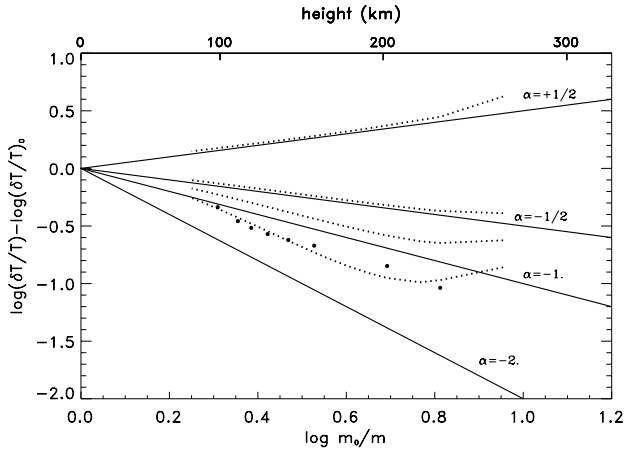

Fig. 8. Comparison between temperature fluctuations derived from observations of granules (*black filled circles*) and those predicted by our method (*dotted lines*) for theoretical exponential models of perturbations (*solid lines*). The fluctuations obtained for granules were shifted upwards by a factor of $|\log(0.015)|$, which would correspond to a perturbation amplitude at height 0 equal to $(\delta T/T)_0 = 0.015$

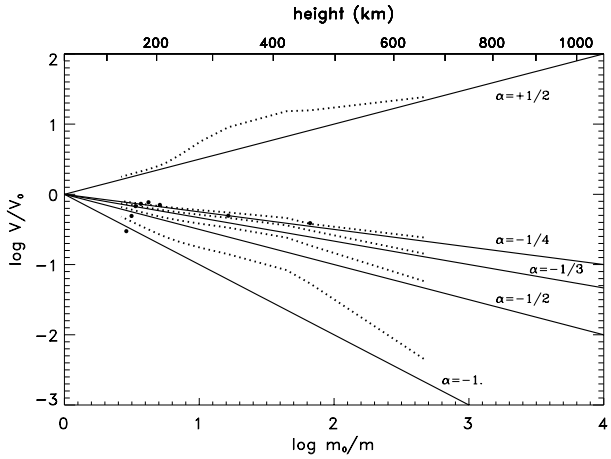

Fig. 9. Comparison between velocity fluctuations derived from observations of granules (*black filled circles*) and those predicted by our method (*dotted lines*) for theoretical exponential models of perturbations (*solid lines*). The fluctuations obtained for granules were shifted upwards by a factor of $|\log(0.49)|$, which would correspond to a perturbation amplitude at height 0 equal to $(\delta V)_0 = 0.49$

the solar photosphere was derived using *RF*s as shown here.

In the present example we deduce temperature and velocity perturbations associated with standard granules. We use the intensity and doppler velocity fluctuations computed by Espagnet et al. (1995) for eight positions measured in the D_2 profile at the following distances $\Delta\lambda$ from the line centre (in Å): 0.108, 0.144, 0.216, 0.252, 0.288, 0.324, 0.360, 0.432. It must be taken into account that only some of these measurements are completely independent whereas the others are obtained by interpolation. Each measurement is therefore influenced by measurements done at other positions in the line and, consequently, involving a range of heights in the atmosphere. This will cause some smoothing in the profiles which is not considered in the method used to derive temperature and velocity fluctuations by using *RF*s for single wavelengths. In order to correct for such an effect, it would be required to convolve the calculated *RF*s with the corresponding spectral bandwidth. Taking into account the instrumental characteristics of the MSDP spectrograph and the interpolation between positions in the line profile, we estimate the effective spectral bandwidth of the data to lie between 0.08 Å and 0.20 Å, according to the location in the 2D field of view.

We calculated average fluctuations over the brightest points of thirteen "typical" granules at the time of maximum brightness, thus assuring the highest signal. By "typical" granules we mean bright, well-defined granules which are not undergoing morphological changes. The associated disturbances of temperature and velocity through the solar photosphere were then calculated with our method. Results are shown as *black filled circles* in Figs. 8 and 9. The height variation of temperature fluctuations is similar to that obtained for an exponential model with $\alpha = -2$ (see Sect. 3.3), after applying a vertical shift of $\log(0.015)$. The corresponding amplitude at height 0, $(\delta T/T)_0$, would then be 0.015.

Altogether, the behaviour of velocity fluctuations with height would not be well described by exponential models of perturbations. Largest disagreement is found at lowest heights, where disturbances of velocity seem to increase rapidly up to a height of ∼150 km. However, the decay that follows this maximum is close to that expected for exponential models with $\alpha = -1/3, -1/4$. The vertical shift which is required to match the granule results with such models in Fig. 9 is equal to $\log(0.49)$, yielding an amplitude at height 0, $(\delta V)_0$, of 0.49 $\mathrm{km\,s^{-1}}$, which is in agreement with values found in the literature (Nesis & Mattig 1989; Vollmöller et al. 1996).

The fluctuations associated with the brightest points of granules represent the amplitude of the spatial distribution of fluctuations that characterizes the granular pattern. The granules themselves as convective cells are better represented by the rms values of spatial fluctuations. Therefore we have computed rms fluctuations of intensity and velocity over the bright central regions of the same granules as above. In order to define the granular cells, we have used an algorithm which finds the borders where the second derivative of brightness equals zero. The area within those limits is what we call the bright region, thus excluding the intergranular space. From the average rms fluctuations made over the whole sample of granules we have derived the expected disturbances of temperature and velocity at different height levels, which should serve as an indication of the rms temperature and velocity within standard granules. Results are shown in Figs. 10 and 11.

The height variation of temperature and velocity is qualitatively similar to that found at the centre of

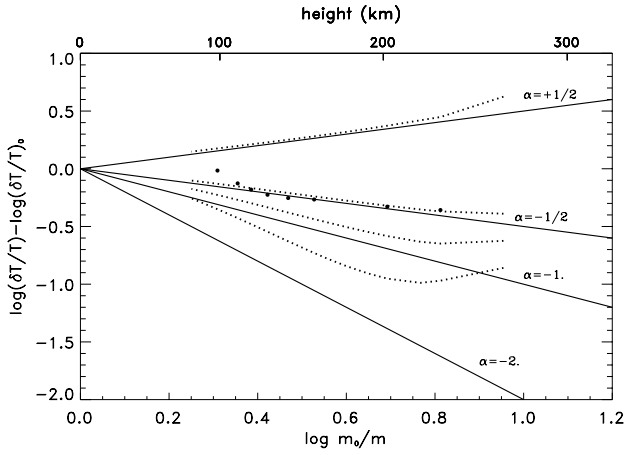

Fig. 10. Results for rms temperature fluctuations. Values derived from observations were shifted upwards by a factor of $|\log(0.008)|$ (see text)

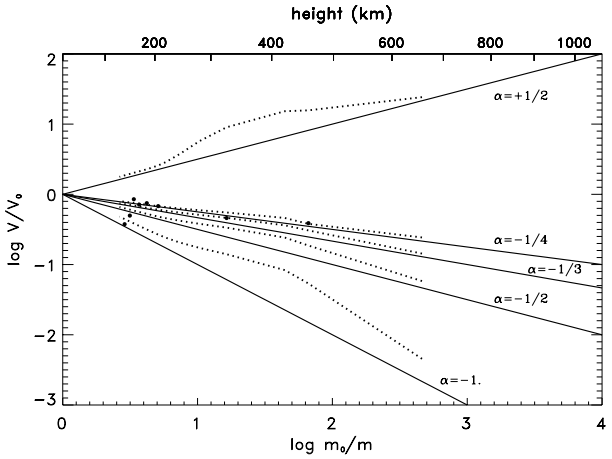

Fig. 11. Results for rms velocity fluctuations. Values derived from observations were shifted upwards by a factor of $|\log(0.51)|$ (see text)

granules. The rms temperature is monotonically decreasing with height and shows two well-distinguished regimes: a steep decay in the low photosphere up to 130 km and a progressively small gradient at larger heights. The rms velocity is seen to increase first from the lowest layers up to 170 km, where an absolute maximum is reached. Above this level the rms velocity decreases rapidly as an exponential function of height. Quantitatively, however, the rms fluctuations are rather different from single values obtained at the centre of granules. By definition, they are systematically smaller. The comparison with exponential models by using logarithmic diagrams in Figs. 10 and 11 show that rms temperature fluctuations (*black filled circles*) are characterized by shallower gradients with height. The vertical shifts which were previously applied to the data to correct for the amplitude at height 0 are of the same order as those used above for results related to granule centres: log(0.008) for rms temperature and log(0.51) for rms velocity.

First attempts to reproduce the vertical structure of solar granulation resulted in several semiempirical models of temperature and velocity fluctuations with height (see review by Bray et al. 1984, and references therein). In the models by Keil & Canfield (1978) and Kneer et al. (1980) for temperature fluctuations, the photosphere is divided in two distinct layers. The rms temperature decreases linearly with a steep gradient below 20–50 km. At this height a discontinuity arises since the vertical gradient becomes almost constant. Although we lack of information for heights below 98 km, our observations show that the decay of temperature fluctuations may be well fitted by exponential functions and that the gradient may be still significant up to larger heights (120 km). Empirical determinations of velocity fluctuations by Keil & Canfield (1978) result in larger gradients between 200–400 km. We note that a systematic shift in height towards upper layers with respect to our results might account for the differences. This is important because it proves that a precise determination of heights is crucial in order to interpret observations. On the other hand, Keil & Canfield's (1978) results are based on observations which are affected by the 5-min oscillations. The granular and oscillatory components of velocity fluctuations are fitted simultaneously in order to reproduce observations. Moreover, the deduced temperature fluctuations involve the combined effects of granules and oscillations. This may also explain discrepancies with our results.

Great progress in the theory of solar granulation has been made recently through numerical simulations. Early work by Steffen et al. (1989) calculated 2-dimensional cylindrical models of solar convection cells, considering only steady state solutions. More realistic 3-D time-dependent numerical simulations have been computed by Stein & Nordlund (1998). A direct comparison between theoretical granulation models and observations is often difficult due to instrumental limitations. Given that models are not affected by seeing or instrumental constraints, they always give higher values for the rms fluctuations in comparison to those which are observed. Apart from the fact that theoretical fluctuations are systematically larger, our results are also in qualitative disagreement mainly because the temperature fluctuations do not show a second maximum in upper layers as predicted by Stein & Nordlund (1998). Contrarily, the derived temperature fluctuations are seen to decrease monotonically with height above the maximum located at deep convective layers.

5. Conclusions

In this work we have calculated Response Functions of the Na I D_1 and D_2 resonance line profiles to temperature and velocity disturbances in the solar photosphere. It has been found that they probe quite different layers in the atmosphere, with $RF_{\rm V}$ extending over larger heights than $RF_{\rm T}$. On this basis we have developed a method to estimate the vertical structure of temperature and velocity perturbations from the observed intensity in the D lines

at several wavelengths. The method performance has been tested with two different kinds of perturbation models: perturbations that behave linearly with depth and perturbations described as exponential functions of depth. Best agreement has been obtained for the linear models since the formulation involved assumes a constant gradient of perturbations with height. Results are also reasonably good for exponential models with small vertical gradients.

By way of illustration, we used an example with a time series of D_2 MSDP spectrograms to study the height variation of solar granulation.

The method we have presented here can be extended to determine other physical parameters, such as the longitudinal component of the magnetic field. Progress in this area will allow investigators to take full benefit of possibilities offered by new solar telescopes.

Acknowledgements. We would like to thank Ch. Coutard, R. Hellier, F. Colson and the Pic du Midi staff for technical assistance during observations. Photometric measurements were done with the microdensitometer "M.A.M.A." of the Institut National des Sciences de L'Univers in Paris. M. T. E. acknowledges financial support from IAC/INSU through a postdoctoral grant.

References

Athay, C., & Canfield, R. C. 1969, ApJ, 156, 695
Babij, B. T., & Stodilka, M. I. 1987, Sol. Danny Bull., 11, 80
Beckers, J. M., & Milkey, R. W. 1975, Sol. Phys., 43, 289
Bellot Rubio, L. R., Ruiz Cobo, B., & Collados, M. 1997, ApJ, 478, L45
Bray, R. J., Loughhead, R. E., & Durrant, C. J. 1984, The Solar Granulation, 2nd edition (Cambridge University Press)
Bruls, J. H. M. J., Rutten, R. J., & Shchukina, N. G. 1992, A&A, 265, 237
Caccin, B., Gomez, M. T., Marmolino, C., & Severino, G. 1977, A&A, 54, 227
Canfield, R. C. 1976, Sol. Phys., 50, 239
Carlsson, M. 1986, A Computer Program for Solving Multi-Level Non-LTE Radiative Transfer Problems in Moving or Static Atmospheres, Report No. 33, Upsalla Astronomical Observatory
Espagnet, O., Muller, R., Roudier, T., Mein, N., & Mein, P. 1995, A&AS, 109, 79
Kelch, W. L., & Milkey, R. W. 1976, ApJ, 208, 428
Keil, S. L., & Canfield, R. C. 1978, A&A, 70, 169
Kneer, F. J., Mattig, W., Nesis, A., & Werner, W. 1980, Sol. Phys., 68, 31
Kneer, F., & Nolte, U. 1994, A&A, 286, 309
Krieg, J. M., Wunnenberg, M., Kneer, F., Koschinsky, M., & Ritter, C. 1999, A&A, 343, 983
Krieg, J., Kneer, F., Koschinsky, M., & Ritter, C. 2000, A&A, 360, 1157
Mein, P. 1971, Sol. Phys., 20, 3
Mihalas, D. 1978, Stellar Atmospheres, 2nd edition (W. H. Freeman, San Francisco)
Nesis, A., & Mattig, W. 1989, A&A, 221, 130
Roudier, T., Eibe, M. T., Malherbe, J. M., et al. 2001, A&A, in press
Ruiz Cobo, B., & del Toro Iniesta, J. C. 1992, ApJ, 488, 462
Sánchez Almeida, J., Ruiz Cobo, B., & del Toro Iniesta, J. C. 1996, A&A, 314, 295
Steffen, M., Ludwig, H.-G., & Krüß, A. 1989, A&A, 213, 371
Stein, R. F, & Nordlund, A. 1998, ApJ, 499, 914
Vernazza, J. E., Avrett, E. H., & Loeser, R. 1981, ApJ, 45, 635
Vollmöller, P., Komm, R., & Mattig, W. 1996, A&A, 306, 294